Journal of Building Engineering 105 (2025) 112433

Contents lists available at ScienceDirect

Journal of Building Engineering

journal homepage: www.elsevier.com/locate/jobe

# Effect of high temperature and cooling method on compression and fracture properties of geopolymer-based ultra-high performance concrete

Junjie Huang, Jun Li, Ruizhe Shao *, Chengqing Wu **

*School of Civil and Environmental Engineering, University of Technology Sydney, Sydney, NSW, 2007, Australia*

ARTICLE INFO

*Keywords:*
GUHPC
High temperature
Cooling method
Mechanical performance
Thermal damage
Microstructural characteristic

ABSTRACT

High-temperature damage to concrete is one of the most common hazards to be experienced during its service life. In this study, the mechanical properties of geopolymer-based ultra-high performance concrete (GUHPC) after high temperature exposure using different cooling methods were investigated. The specimens were heated to 200 °C, 400 °C, 600 °C, 800 °C and 1000 °C, followed by air and water cooling. Then the quasi-static tests were conducted with the assistance of a digital image correlation (DIC) device to examine the compressive and flexural strength, elastic modulus, fracture performance, and failure patterns. In addition, the microstructural change of GUHPC after high temperature exposure was analysed utilizing X-ray Diffraction (XRD) and Scanning Electron Microscope (SEM) methods. Test results revealed that GUHPC demonstrated different degrees of thermal damage at high temperatures ranging between 200 °C and 1000 °C but exhibited superior thermal spalling resistance. The reduction in strength, elastic modulus and fracture properties after high temperature exposure can be divided into three stages, i.e., 25–200 °C, 400–600 °C and 800–1000 °C, respectively. These three stages defined the mild, moderate, and severe damage. Compared to air cooling, water cooling caused thermal shock to specimens, resulting in a greater loss of strength. The microstructural analysis indicated that the damage to steel fibres along with the formation of new substances due to phase transition at high temperatures led to variations in the internal structure, consequently affecting the mechanical performance of the studied GUHPC.

## 1. Introduction

Engineering structures are subjected to a wide range of challenges during the lifespan. The challenges include a range of natural hazards including earthquakes, hurricanes, tsunamis, and fires, as well as man-made hazards such as impacts and explosions. These hazards may even occur simultaneously and further jeopardize the structural safety. To achieve a deeper comprehension of structural responses to extreme events, it is essential to explore the mechanical properties of building materials in such circumstances.

The development of cement-based ultra-high performance concrete (CUHPC) is a topic of much interest in current construction and infrastructure sectors. It's a promising building material with many outstanding properties that bring a number of compelling

* Corresponding author. School of Civil and Environmental Engineering, University of Technology Sydney, NSW, 2007, Australia.
** Corresponding author. School of Civil and Environmental Engineering, University of Technology Sydney, NSW, 2007, Australia.
*E-mail addresses:* Ruizhe.shao@uts.edu.au (R. Shao), Chengqing.wu@uts.edu.au (C. Wu).

https://doi.org/10.1016/j.jobe.2025.112433
Received 10 January 2025; Received in revised form 11 March 2025; Accepted 19 March 2025
Available online 20 March 2025

advantages over conventional concrete, and good for structures against multi-hazards [1–3]. However, with the fast growth of infrastructure, the environmental impact of civil engineering has come to the fore. The demand to reduce the use of cement in concrete production is rising as awareness of the environmental issues caused by the $CO_2$ produced during cement production growth. Cement industry is accountable for 7 % of the world's total $CO_2$ emissions [4]. In this context, geopolymer-based UHPC (GUHPC) is developed which replaces cement with geopolymer as the binder. Geopolymers are inorganic binders formed by a chemical reaction of the aluminosilicate materials, which originate from industrial by-products with less environmental impact as compared to Portland cement [5,6]. Previous studies have primarily focused on normal strength geopolymer concrete [7,8]. In recent years, there has been growing interest in high strength geopolymer concrete, but research on its fire resistance still remains limited [9–12].

Studies have indicated that at exposure temperatures in excess of 200 °C, geopolymer slurries, mortars, and concrete exhibited superior performance regarding the thermal integrity and residual strength in comparison with traditional Portland cement concrete (PCC) [13–16]. The notable temperature tolerance is attributed partially to the fact that geopolymers do not include the feldspar phase containing $Ca(OH)_2$. At a critical temperature of about 400 °C, the cement matrix begins to decompose, interfacial damage intensifies, and cracks expand, resulting in a sharp decline in mechanical properties and potential spalling. Moreover, the microstructure of PCC is destroyed by the dehydroxylation of $Ca(OH)_2$, leading to extensive vaporisation [17–19]. Zhang et al. [20] further studied the mechanical behaviour of calcium silicate hydrate (C-S-H) under elevated temperatures and found that high temperatures alter the shear behaviour of C-S-H particles, affecting both the shear modulus and shear strength. These changes at the nanoscale contributed to thermal shrinkage, pore structure modifications, and crack propagation at the macroscale, ultimately leading to the degradation of the overall strength of cementitious composites. Previous investigations have pointed out that the degradation of high-strength concrete was more severe in high-temperature environments as compared to that of ordinary concrete [21,22]. It has been illustrated that CUHPC suffers explosive spalling when subjected to temperatures exceeding 400 °C. The spalling of UHPC at high temperatures is mainly driven by thermal stress, with vapor pressure accelerating the process [23]. This behaviour is more pronounced in CUHPC than in PCC, primarily due to its compact microstructure, which leads to the accumulation of internal pore pressures that cannot be adequately released [24,25]. This suggests that despite similar underlying mechanisms, variations in strength result in distinct differences in concrete performance after high-temperature exposure.

Studies have revealed that the cooling methods greatly influence the characteristics of concrete experiencing high temperatures due to thermal stress [26]. The different cooling regimes may cause secondary damage to heated concrete and increase the risk of injuries on site. Especially with rapid cooling, this may exacerbate microcrack development within concrete under high/extreme-temperature conditions, leading to severe structural damage [27,28]. Researchers compared concretes cooled by water and natural cooling, and it was commonly observed that the natural cooling maintained relatively higher residual mechanical properties [29,30]. It was also reported that before 400 °C, air-cooled specimens demonstrated lower strength than water-cooled specimens. However, as the temperature further increased, the strength of the water-cooled specimens reduced signally [31]. Further research into the dynamic properties of geopolymer-based high performance concrete (GHPC) revealed that a high cooling rate in water generated the remarkable thermal shock, leading to secondary damage to the concrete matrix [32].

Despite the superior heat and fire resistance of geopolymer concrete [13,33]. For now, several studies have explored the thermal degradation mechanisms of geopolymer concrete [34]. However, unlike conventional geopolymer concrete, GUHPC is a fine-grained composite without coarse aggregates. Its denser matrix, lower permeability, and fibre incorporation lead to unique failure mechanisms, fracture behaviour, thermal degradation characteristics, and spalling tendencies. The existing research lacks a systematic study on fracture toughness at elevated temperatures, and the influence of different cooling methods on the residual mechanical properties of GUHPC remains unexplored, despite its critical impact on post-fire performance. Therefore, this study evaluates the mechanical properties of GUHPC after elevated temperature exposure following varying cooling regimes. In the experiment, GUHPC was subjected to 200 °C, 400 °C, 600 °C, 800 °C and 1000 °C. After heating, specimens were cooled to ambient temperature utilizing air and instant water cooling. Subsequently, the static mechanical tests were conducted with the assistance of digital image correlation (DIC), and the strength, elastic modulus, fracture energy, and toughness were investigated in detail. Additionally, this study compared the heated GUHPC specimens with untreated cases, and systematically explored the effect of elevated temperatures on GUHPC behaviour in the micro levels using XRD and SEM methods.

## 2. Experimental tests

### 2.1. Material and preparation

Previous research indicates that combining fly ash (FA) and ground blast furnace slag (GGBFS) as a geopolymer binder is a better option as compared to using a single material [35,36]. In the current study, FA and GGBFS were selected as geopolymer binder for the

**Table 1**
Chemical compositions (%) and physical properties of GGBFS, FA, and SF.

| Materials | $SiO_2$ | $Al_2O_3$ | $Fe_2O_3$ | CaO | MgO | $SO_3$ | LOI | Density (kg/m$^3$) | PS (μm) |
|---|---|---|---|---|---|---|---|---|---|
| GGBFS | 26.0 | 14.0 | 0.4 | 44.0 | 8.0 | 3.0 | 0.3 | 3100 | 5–30 |
| FA | 54.0 | 23.0 | 0.5 | 12.0 | 0.4 | 0.8 | 1.3 | 2500 | 1–100 |
| SF | 92.0 | 0.8 | 1.3 | 0.3 | 0.8 | 0.2 | 2.1 | 2200 | <1 |

Note: LOI refers to loss on ignition and PS denotes particle size.

preparation of GUHPC. The chemical compositions of GGBFS, FA and silica fume (SF) are given in Table 1. The geopolymer binders were activated utilizing NaOH and $Na_2SiO_3$ solutions. The microstructure of GUHPC was optimised denser via utilizing the quartz sand instead of conventional coarse aggregate. Water was incorporated to enhance mixture workability, achieving better performance. Moreover, straight steel fibres with a volume content of 1.5 %, measuring 8 mm in length and 0.12 mm in diameter were utilized, and their properties are listed in Table 2. Table 3 shows the mix proportions of the studied GUHPC. The compressive test utilized 50 mm cubic specimens, while the three-point bending test used 40 × 40 × 160 mm prisms.

### 2.2. Test setup

#### 2.2.1. Heating rate and cooling method

An electric furnace that can heat up to 1300 °C as shown in Fig. 1(a) was used to heat specimens to five designated temperatures of 200 °C, 400 °C, 600 °C, 800 °C, and 1000 °C. Prior to heating, the specimens was cured for 28 days. A slow heating rate could help to decrease the thermal difference between the interior and exterior of concrete, facilitated gradual moisture release within its matrix. This helped to maintain the stability of matrix and reduced the probability of spalling. In this study, the heating rate was controlled at 4 °C/min [37]. To ensure uniform temperature distribution within the specimen, the target temperature was maintained for additional 2 h after being reached [38,39], as depicted in Fig. 2. Additionally, the chosen specimen sizes (40 × 40 × 160 mm and 50 × 50 × 50 mm) were selected in part to facilitate efficient heat transfer, reducing the likelihood of significant internal temperature gradients. The small cross-sectional sizes of the specimens allowed for more even heating as compared to larger concrete elements, improving temperature consistency. Due to the presence of steel fibres, the heat transfer rate of GUHPC is higher than that of PCC [40].

Natural cooling and water cooling were employed for the subsequent cooling phase. Natural cooling involved placing the heated specimens in a chamber for 24 h until cooling down to ambient temperature. This method simulated the gradual cooling of GUHPC in a natural environment. In addition, water cooling was performed via placing specimens in the pre-prepared buckets of water as shown in Fig. 1(b). The cooling duration in water was 12 h, then specimens were dried in the ambient environment for another 12 h, followed by mechanical and microstructural tests. This method can simulate a fire scenario where the firefighters intervene to extinguish the blaze and rapidly cool down the concrete structure.

#### 2.2.2. Uniaxial compression test

To study the performance of GUHPC under static compressive loading, the specimens were tested utilizing Shimadzu Universal Testing Machine UH500 in accordance with ASTM C109/C109M [41]. The loading was controlled by a displacement regime with a rate of 0.2 mm/min. DIC system was fitted to the front of the machine to collect strain data in real time and determine the elastic modulus. Fig. 3 displays the compressive test setup.

#### 2.2.3. Flexural behaviour

This study focuses on the fracture mechanical properties of GUHPC due to their critical role in complex stress state, capability to capture crack propagation, and effectiveness in evaluating the high-temperature mechanical performance. Fig. 4(b) displays the three-point bending test setup in accordance with ASTM C78 [42]. Prism specimens were notched at the bottom of mid-span by a grinder with a width of 1 mm and a depth of 5 mm as shown in Fig. 4(a). The beam specimens were tested using Shimadzu Universal Testing Machine AGX50 with a displacement loading rate of 0.02 mm/min. DIC device was also fitted to the front of the machine to collect crack mouth opening displacement (CMOD) in real time.

#### 2.2.4. Microstructural test

XRD is a characterization technique for analysing the microstructure of substances. The Bruker D8 Discover diffractometer was used to analyse the formation of the crystal phase and phase transformation of the sample with a 2θ ranging between 5 and 70°. Subsequently, the coated samples were fixed with carbon conductive tape, followed by examining their microstructural patterns before and after heating using Zeiss-EVO-LS15 SEM device. The XRD machine and SEM machine are as Fig. 5 shown.

## 3. Test results and discussion

### 3.1. Material performance after high temperature

#### 3.1.1. Appearance changes in specimens

Fig. 6 illustrates the appearance changes in the GUHPC specimens after thermal exposure. The colour of the specimens at 25 °C and after 200 °C was similar. At 400 °C, the colour began to get darken and took on a light brownish-pink colour. When the temperature rose to 600 °C, the colour became the darkest, with a hint of the brownish pink. At 800 °C and 1000 °C, the colour of the test pieces

**Table 2**
Properties of steel fibres.

| Length (mm) | Diameter (mm) | Tensile strength (MPa) | Young's Modulus (GPa) | Density (kg/m$^3$) |
|---|---|---|---|---|
| 8 | 0.12 | 3300 | 210 | 7850 |

**Table 3**
Mixing proportions of GUHPC (kg/m$^3$).

| GGBFS | SF | FA | Alkali activator | Quartz sand | Water | Steel fibre |
|---|---|---|---|---|---|---|
| 1000 | 80 | 150 | 543 | 1060 | 81 | 117.0 |

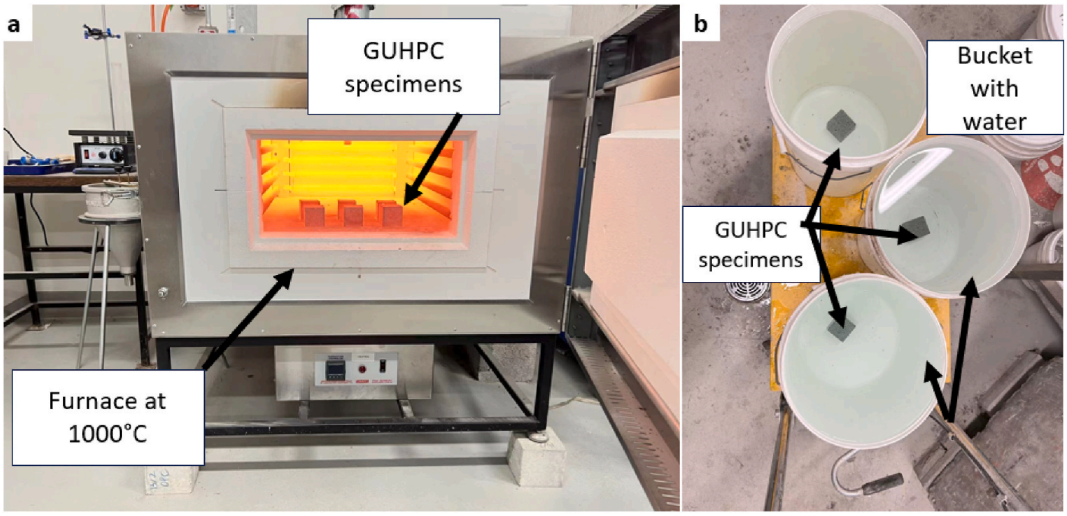


**Fig. 1.** (a) Specimens heated in furnace and (b) water cooling method.

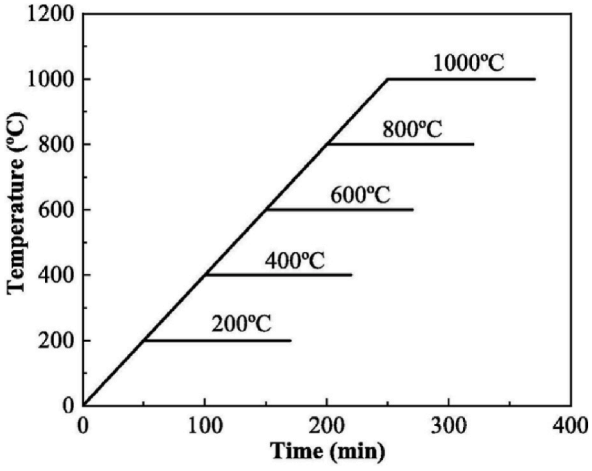


**Fig. 2.** Heating rate of GUHPC.

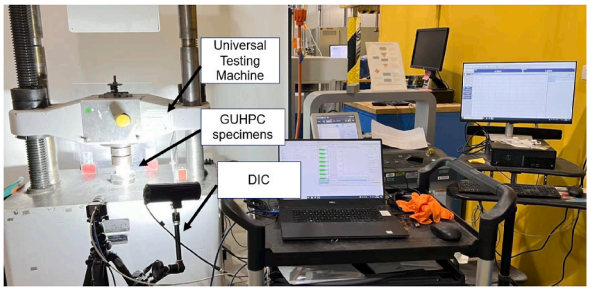


**Fig. 3.** Compressive test setup and fitted DIC device.

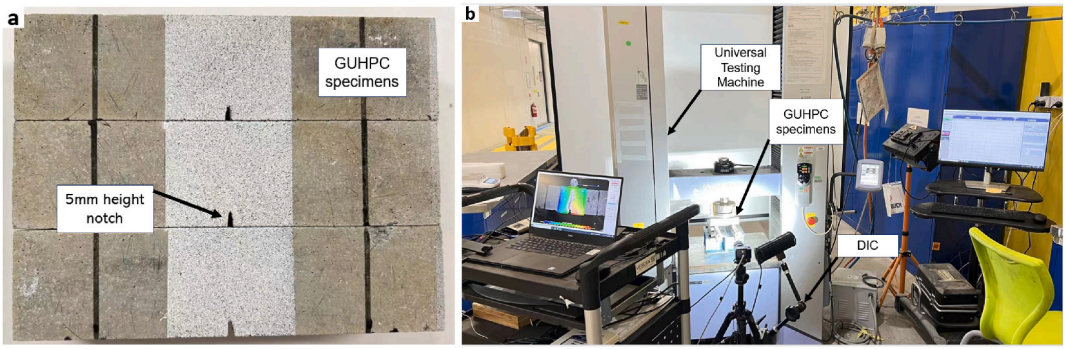


**Fig. 4.** (a) GUHPC notched prismatic specimens and (b) three-point bending test setup.

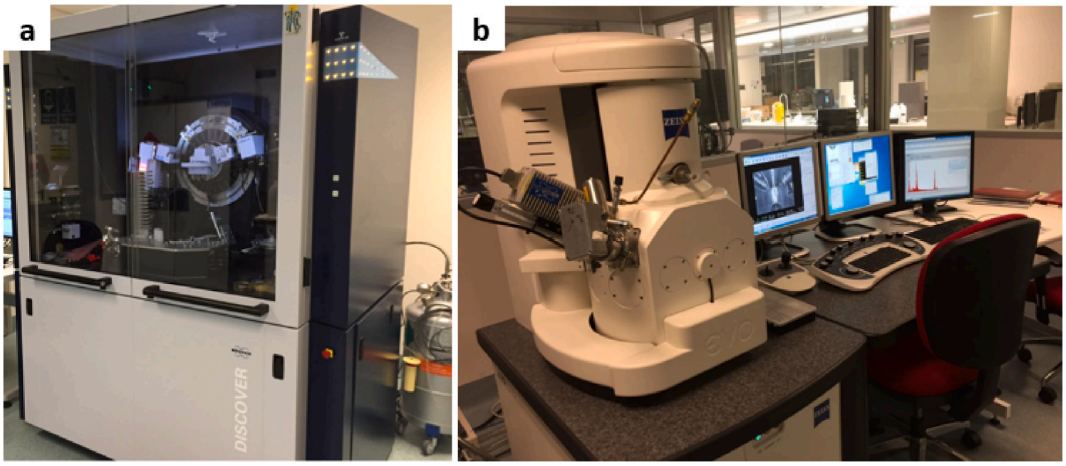


**Fig. 5.** (a) Bruker D8 Discover diffractometer and (b) Zeiss-EVO-LS15 SEM apparatus.

gradually became lighter. The 800 °C test pieces started to turn greyish white and the 1000 °C pieces were the lightest, with an overall greyish white colour. It is noteworthy that the different cooling methods seem not to affect the colour changes. The alteration in hue of geopolymer concrete when subjected to high temperatures primarily stems from its FA component. FA, a by-product of coal combustion, contains various minerals and compounds that are susceptible to chemical metamorphoses at elevated temperatures [43]. In addition, at elevated temperatures, FA and GGBFS, which contain minerals such as aluminium, calcium, and iron, are prone to undergo oxidation reactions that induce colour changes in the concrete matrix. Specifically, the oxidation of iron leads to a formation of reddish-brown or darker hue, thereby deepening the colouration of the concrete. Moreover, at high temperatures, the evaporation of water and organic contaminants in geopolymer materials can alter their appearance, frequently manifesting as either lighter or darker shades. Additionally, the presence of alkaline constituents within geopolymer concrete may lead to the formation of white or pale residues on its surface upon exposure to high temperatures, imparting a lighter or whitish appearance to the concrete.

In terms of crack development, there is no evident difference between water-cooled and naturally cooled specimens as observed by the naked eye. At low temperatures, the surface of test pieces did not demonstrate any cracks. However, after reaching 600 °C, tiny cracks began to spread around the small holes, and the length and depth of the cracks were relatively small. When it reached 800 °C and 1000 °C, visible cracks appeared, with increasing width and depth. Meanwhile, these cracks exhibited regularity and began to extend and develop from many small holes that originally existed. It should be noted that none of the pieces exhibited any signs of spalling, which indicated that geopolymer concrete had strong resistance to thermal spalling.

### *3.1.2. Mass loss of specimens*

Concrete commonly loses mass when exposed to heat. This pattern of mass loss largely reflects changes in the internal structure of concrete. For a deeper understanding of this phenomenon, a measurement in mass loss was made on GUHPC from the experimental group at different temperatures. Fig. 7 shows the effect of cooling method and temperature on GUHPC mass loss. The mass variations in specimens were determined after completely cool and dry. After water cooling, GUHPC samples contained residual moisture that was not inherent to the material itself. Thus, before conducting the mass measurement, it is recommended to ensure that any residual moisture inside the concrete evaporates completely.

The mass loss of GUHPC under both cooling conditions was relatively small at 200 °C, which was primarily attributed to the loss of

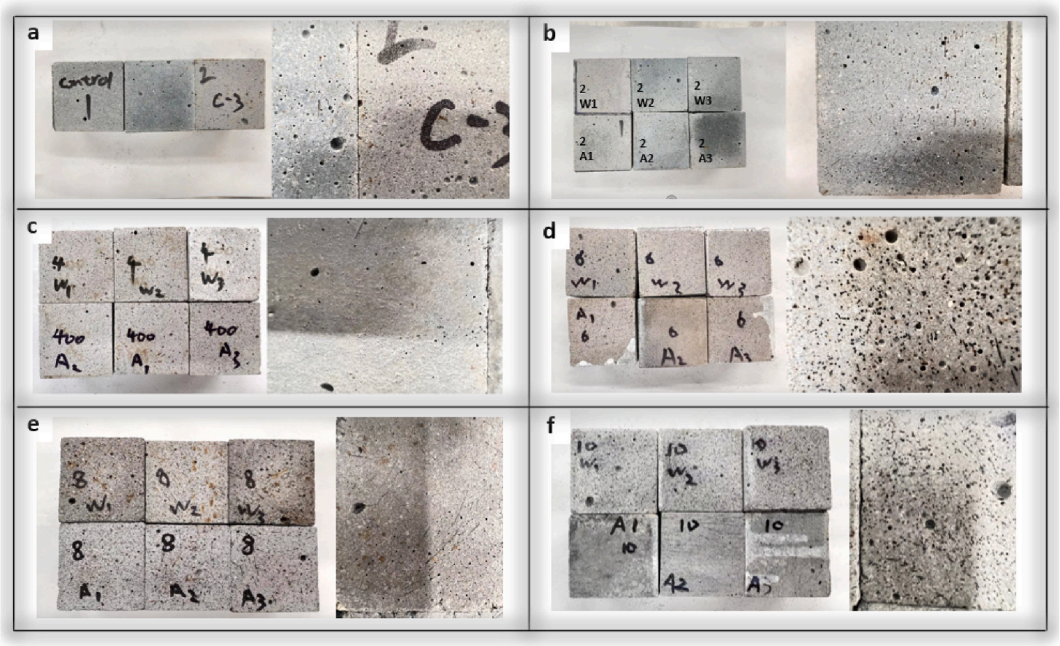


**Fig. 6.** GUHPC specimens after (a) 25 °C, (b) 200 °C, (c) 400 °C, (d) 600 °C, (e) 800 °C, and (f) 1000 °C temperature exposure and cooling down.

water and volatile substances [44]. As the temperature rose to 400 °C, air-cooled specimens' mass loss rate increased sharply, which indicated that the hydration products and organic substances in the geopolymer began to decompose in large quantities [45]. As expected, the water-cooled samples exhibited a larger and increasing mass loss in the same temperature, suggesting that air cooling helped to protect the structural integrity of material. When the temperatures varied between 400 °C and 800 °C, the mass loss continued to increase slowly for both, but the rate of increase for the air-cooled samples was still lower than that of the water-cooled samples, possibly because the air cooling provided a milder temperature gradient and better thermal stability. In a higher temperature phase between 800 °C and 1000 °C, the rate of mass loss for both methods reduced, probably because the decomposition of some components, such as $CaCO_3$, completed, leaving no further components capable of volatilization within this thermal band [46].

### 3.2. Compressive performance

#### 3.2.1. Compressive strength

Table 4 compares the compressive strength of GUHPC at different temperatures with two cooling methods. GUHPC exhibited a

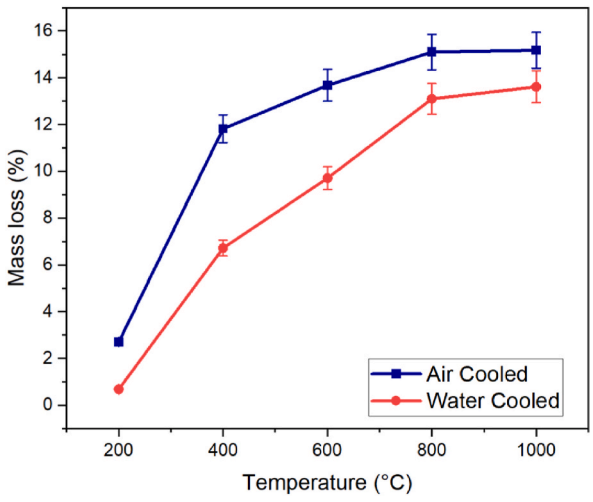


**Fig. 7.** Mass loss rate of GUHPC after air cooled and water cooled.

standard compressive strength of 138.6 MPa at room temperature. As temperature gradually increased, strength began to decline for specimens subjected to both cooling methods. The strength of GUHPC exhibited three distinct phases after high temperatures, starting with the room temperature and 200 °C phases. At 200 °C exposure, the compressive strengths were 128 MPa for air cooling method and 123 MPa for water cooled, respectively, and the corresponding residual strength percentages were 92.4 % and 88.7 %, respectively. The second stage ranged from 400 °C to 600 °C. At 400 °C, the strengths yielded 92.2 MPa and 86.7 MPa with the residual percentages of 66.5 % and 62.6 %, respectively. At 600 °C, the strengths were 71.2 MPa and 66.6 MPa with the residual percentages of 51.4 % and 48.1 %, respectively, indicating a remarkable reduction. The third stage varied between 800 °C and 1000 °C, where strength degradation was the most evident. At 800 °C, the strengths from air and water cooling were only 19.7 MPa and 17.9 MPa, with only 14.2 % and 12.9 % being left. At 1000 °C, the strengths were even lower, reaching 10.6 MPa and 9.1 MPa, respectively, with the residual ratios of only 7.6 % and 6.6 %, demonstrating that the compressive capacity of GUHPC suffered severe damage at extreme temperatures. This decline was likely ascribed to the formation of new micro-pores inside the specimens resulted from the volatilization of carbon in FA and decomposition of geopolymer gel [43]. Between 800 and 1000 °C, the strength decreased at a slower rate. The key factor was the refractory materials including FA and GGBFS added into GUHPC. In addition, the sintering reaction of unreacted FA contributed to improving the GUHPC strength after 800 °C high temperatures [45].

Fig. 8 reveals a three-stage trend on the strength of GUHPC under the different cooling methods. Stage I started from 25 °C to 200 °C, when the difference between these two cooling regimes was 3.9 %. Stage II covered 400 °C and 600 °C, where the difference was 6.6 % and 6.5 %, respectively. Stage III was between 800 °C and 1000 °C with the differences of 9.1 % and 14.2 %, respectively. Notably, water cooling induced thermal shock, but the difference in compressive strength was insignificant as compared to air cooling, with variations no more than 10 % below 800 °C. The highest difference within the two methods was observed in the case of 1000 °C, which was a result of the severe damage caused by thermal shock due to extreme temperatures as well as hydration damage from CaO in GGBFS during water cooling. Hence, it was inferred that the difference was not remarkable despite the notable strength loss of GUHPC by water cooling. Compared to GUHPC, the difference in cooling methods for CUHPC at high-temperature was higher [47], indicating that GUHPC had a superior resistance between different cooling regimes and a high resistance to thermal shock.

Fig. 9 shows the residual stress-strain curves of GUHPC. The stiffness of GUHPC demonstrated a significant decline as the temperature rose, and the strain at the peak stress became larger, implying that the toughness of concrete decreased under the action of high temperatures.

Fig. 10 compares the normalised compressive strength of different concretes with air cooling after high temperature [32,48]. Regardless of geopolymer-based ordinary concrete (GC), geopolymer-based high strength concrete (GHPC), or GUHPC, the declining trend after high temperatures was essentially consistent with the foregoing three decline stages. Moreover, the geopolymer-based concrete with higher strengths exhibited a more evident loss in compressive strength, which could be ascribed to the inherently denser matrix designed for greater strength. The compactness raised the pore size when subjected to high temperatures, inducing the alterations at both the mesoscopic and macroscopic levels. Consequently, the expansion within the pore network evidently undermined its compressive strength.

To assess the safety of geopolymer concrete in high-temperature environments, the degradation model of compressive strength for GUHPC subjected to different temperatures is proposed as follows:

$$f_r = \frac{f_i}{1 + a \times \left(\frac{T-25}{1000}\right)^b} \tag{1}$$

where fi is the compressive strength of GUHPC at the ambient temperature; $a$ and $b$ are the fitting parameters; $T$ is the target temperature and fr is the residual compressive strength of GUHPC after high temperatures. Fitting parameters, $a$ and $b$ were obtained by fitting experimental data. The values of these two parameters will vary depending on the experimental data, concrete mixture, and fibre type. Parameter

$a$ quantifies the extent to which temperature influences the residual strength of the material. A larger value indicates a more pronounced impact of temperature variations on residual strength. Conversely, parameter $b$ controls the non-linearity of temperature effect on residual strength. It determines whether the relationship between the residual strength and temperature change is linear or exhibits complex non-linear behaviours, such as a rapid decline in residual strength with an increase in temperature. Fig. 11 displays the fitting curves of the experimental data, and the parameter values are listed in Table 5.

**Table 4**
Compressive strength of GUHPC at elevated temperatures.

| Temperature (°C) | $\sigma_{AC}$ (MPa) | $\sigma_{WC}$ (MPa) | $RS_{AC}$ (%) | $RS_{WC}$ (%) | CMD (%) |
|---|---|---|---|---|---|
| 25 | 138.6 | 138.6 | 100.0 | 100.0 | 0.0 |
| 200 | 128.0 | 123.0 | 92.4 | 88.7 | 3.9 |
| 400 | 92.2 | 86.7 | 66.5 | 62.6 | 6.0 |
| 600 | 71.2 | 66.6 | 51.4 | 48.1 | 6.5 |
| 800 | 19.7 | 17.9 | 14.2 | 12.9 | 9.1 |
| 1000 | 10.6 | 9.1 | 7.6 | 6.6 | 14.2 |

Note: $\sigma_{AC}$ is air cooled compressive strength; $\sigma_{WC}$ is water cooled compressive strength; $RS_{AC}$ is air cooled residual strength percentage; $RS_{WC}$ is water cooled residual strength percentage; CMD is cooling method difference percentage.

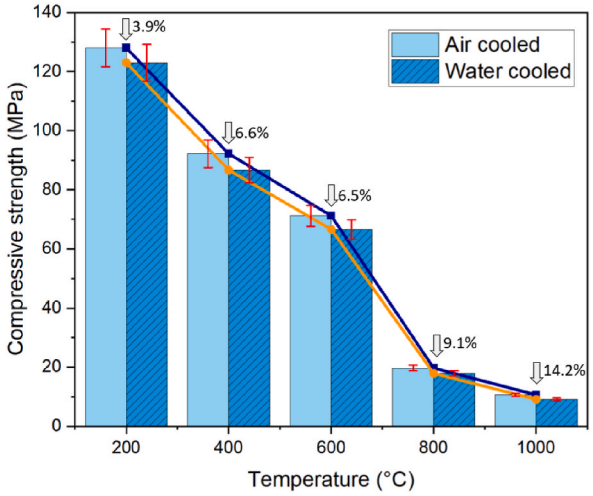


**Fig. 8.** Comparison of compressive strength between different cooling regimes.

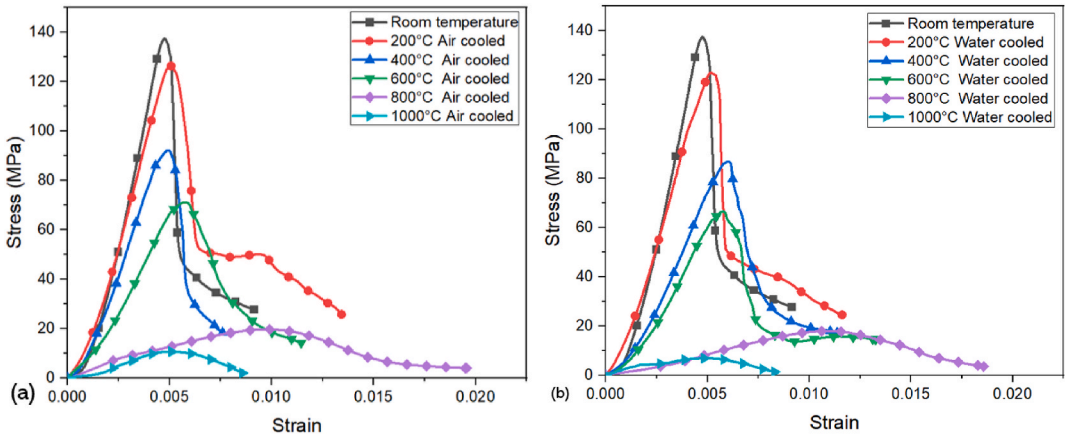


**Fig. 9.** Stress-strain curves of GUHPC with (a) air cooling (b) water cooling method.

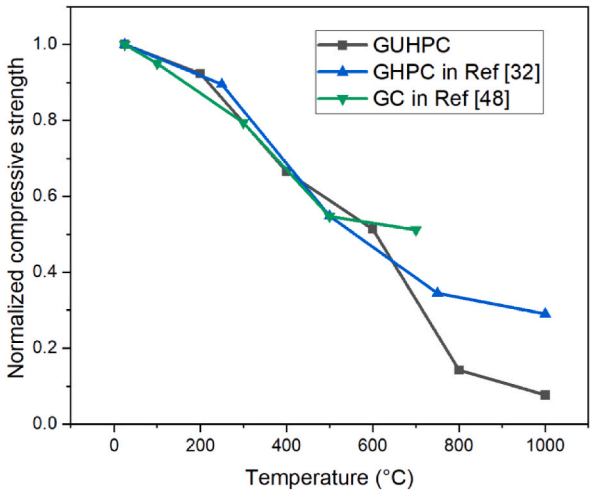


**Fig. 10.** Normalised strength of different concretes after high temperatures with air cooling.

GUHPC and CUHPC exhibit distinct compressive strength degradation characteristics under thermal exposure, each exhibiting advantages at different temperature stages [49]. CUHPC follows a rise-then-decline trend in compressive strength, rendering it perform better than GUHPC at lower temperatures, such as 200 °C. However, as the temperature increases further, GUHPC exhibits better residual strength retention. For instance, at 400 °C, GUHPC still retains 66.5 % of its original strength, while CUHPC drops to 56.9 %. Additionally, CUHPC requires extra fibre reinforcement to maintain its structural integrity beyond 400 °C, whereas GUHPC has no explosive spalling even without fibre reinforcement. This suggests that GUHPC has better thermal degradation resistance, while CUHPC relies more on fibre addition to improve its high-temperature performance. Furthermore, GUHPC exhibits significantly lower sensitivity to different cooling methods compared to CUHPC [50]. In CUHPC, water cooling causes a notable strength loss, with a difference of 15.2 % as compared to natural cooling at 500 °C. In contrast, GUHPC maintains more stable strength under different cooling conditions, with differences of only 6.5 % at 600 °C and 14.2 % at 1000 °C, remaining below 15 %. These comparisons indicate that GUHPC possesses superior performance after high-temperature exposure and rapid cooling. In comparison, CUHPC is more susceptible to cooling-induced strength degradation, demonstrating its higher sensitivity to cooling methods.

### 3.2.2. Elastic modulus of GUHPC

The elastic modulus was determined by taking the slope between the two points of the linear risen area in the stress-strain curve as depicted in Fig. 9. The elastic modulus at ambient temperature correlated to 30–70 % of peak stress. However, at an elevated temperature of 1000 °C, this range diminished to 10–30 %, which was mainly because the heightened thermal condition adversely affected the peak stress of GUHPC. Table 6 lists the elastic modulus of GUHPC after thermal exposure. The relationship between compressive strength and elastic modulus at different temperatures with two cooling methods is exhibited in Fig. 12. Both the compressive strength and elastic modulus decreased as the temperature increased, and the declining trend of two variables was essentially identical. This indicated that the elastic modulus of GUHPC was affected by temperature in the same way as compressive strength. Notably, the cooling method appeared to negligibly influence these properties.

In contrast with CUHPC, GUHPC exhibits a lower elastic modulus [51]. Studies [52] have demonstrated that the elastic modulus of GUHPC with above 150 MPa was more than 30 GPa, while that of CUHPC with above 100 MPa was more than 35 GPa [53,54]. According to the research, several empirical equations have been proposed for cement-based concrete. Fig. 13 shows the relationship between the elastic modulus and compressive strength for GUHPC. Table 7 lists the empirical formulas for different concretes. As shown in Fig. 13, the empirical equations for cement-based concrete overestimated the elastic modulus for GUHPC. Therefore, a new empirical equation was proposed in Eq. (2). The proportionality constant of Eq. (2) was notably lower in comparison with that for PCC and CUHPC. This indicates that the correlation between compressive strength and elastic modulus for GUHPC differs from that of PCC and CUHPC. This finding aligns with previous observations on other geopolymer concretes [55,56].

$$E = 3.6 \times \sqrt{f_c} \ (E \text{ in GPa}, f_c \text{ in MPa}) \tag{2}$$

In addition, according to the results in this study, the elastic modulus of GUHPC at elevated temperature was fitted as the method exhibited in Fig. 13. The empirical formula under different temperatures and cooling methods is proposed as follows, with the value of the temperature coefficient $a$ listed in Table 8.

$$E = 3.6a \times \sqrt{f_c} \tag{3}$$

### 3.2.3. Failure patterns

Typical compressive failure patterns of GUHPC after high temperatures are shown in Figs. 14 and 15. The specimens showed more damage under water cooling than air cooling, as thermal shock further weakened the heated concrete's internal structure. The markedly increase in damage cracks highlighted the potentially severe impact of water cooling, which contributed to a pronounced

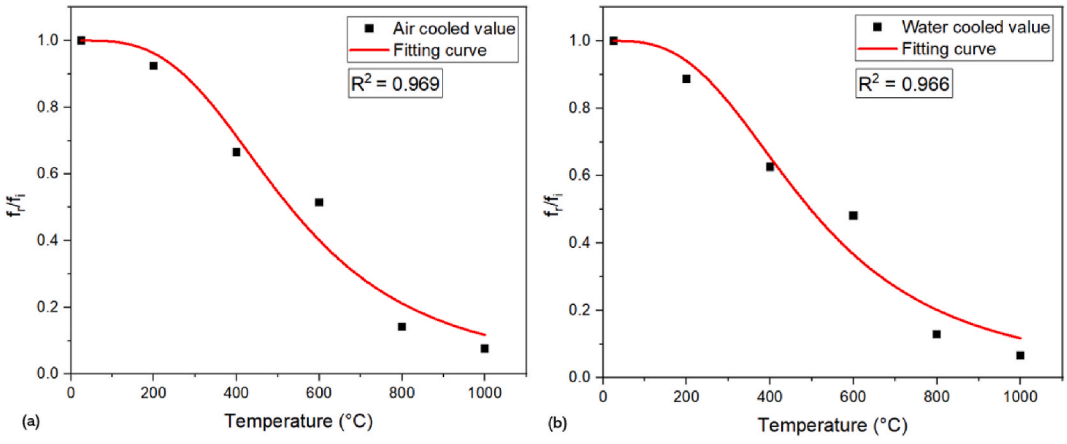


**Fig. 11.** Degradation model of compressive strength after (a) air cooled and (b) water cooled.

**Table 5**
Values for fitting parameters.

| Parameter | Air cooled | Water cooled |
|---|---|---|
| a | 10.10 | 9.43 |
| b | 3.68 | 3.26 |

**Table 6**
Elastic modulus of GUHPC after high temperature exposure.

| Temperature (°C) | $E_{AC}$ (GPa) | $E_{WC}$ (GPa) | $RM_{AC}$ (%) | $RM_{WC}$ (%) | CMD (%) |
|---|---|---|---|---|---|
| 25 | 40.9 | 40.9 | 100.0 | 100.0 | 0.0 |
| 200 | 32.9 | 31.3 | 80.4 | 76.5 | 4.9 |
| 400 | 25.9 | 23.6 | 63.3 | 57.8 | 8.9 |
| 600 | 19.6 | 18.8 | 47.9 | 46.0 | 4.1 |
| 800 | 5.0 | 4.6 | 12.2 | 11.2 | 8.0 |
| 1000 | 3.7 | 3.0 | 9.0 | 7.3 | 18.9 |

Note: $E_{AC}$ is air cooled elastic modulus; $E_{WC}$ is water cooled elastic modulus; $RM_{AC}$ is air cooled residual elastic modulus percentage; $RM_{WC}$ is water cooled residual elastic modulus percentage; CMD is cooling method difference percentage.

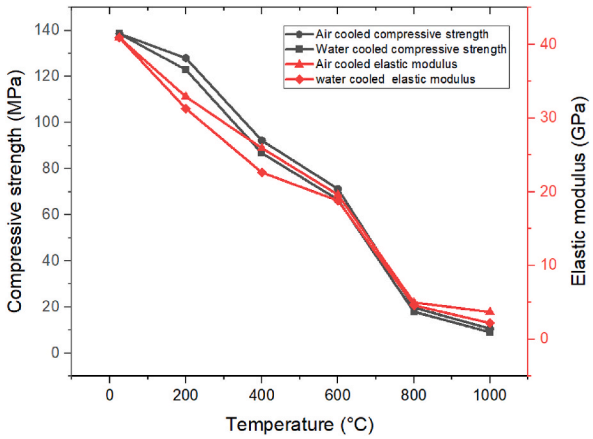


**Fig. 12.** Effect of temperature and cooling method on elastic modulus of GUHPC.

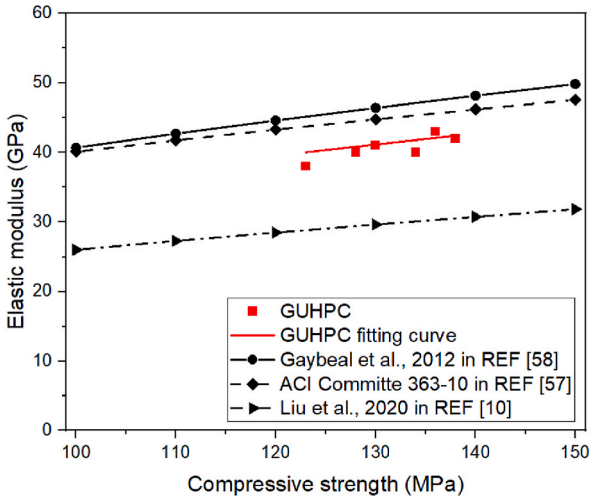


**Fig. 13.** Correlation between compressive strength and elastic modulus of concretes.

**Table 7**
Empirical equations of elastic modulus for different concretes. ($E$ in GPa, $fc$ in MPa).

| Standard/Researchers | Equations |
|---|---|
| ACI 363R [57] | $E = 3.32 \times \sqrt{f_c} + 6.9$ |
| Gaybeal et al. [58] | $E = 3.84 \times \sqrt{f_c}$ |
| Liu et al. [10] | $E = 2.6 \times \sqrt{f_c}$ |

**Table 8**
Value for empirical formula of elastic modulus of GUHPC after high temperatures.

| Temperature (°C) | Air cooled | Water cooled |
|---|---|---|
| 200 | 0.80 | 0.78 |
| 400 | 0.74 | 0.70 |
| 600 | 0.65 | 0.63 |
| 800 | 0.32 | 0.30 |
| 1000 | 0.28 | 0.27 |

deterioration of GUHPC when subjected to high temperatures.

### 3.3. Flexural behaviour

#### 3.3.1. Flexural strength

Fig. 16 illustrates the variations in flexural strength of GUHPC under different cooling methods. The air-cooled specimens at 200 °C decreased to 14.2 MPa and that of the water-cooled specimens was 12.9 MPa, with the residual strength percentages of 88.2 % and 80.1 %, respectively. At 400 °C and 600 °C, both cooling methods resulted in a remarkable decline in flexural strength, with residual percentages of 72.7 % and 49.1 % for air-cooled cases and 50.9 % and 41.6 % for water-cooled cases, respectively. The flexural strength decreased significantly at 800 °C and 1000 °C, only 2.2 MPa and 0.8 MPa at 1000 °C, respectively. Table 9 lists the detailed flexural strength and changes of GUHPC at various temperatures. Water cooling affected flexural strength more significantly than compressive strength. At 400 °C, the thermal shock caused by the water cooling resulted in a flexural strength of almost 30 % lower than air cooling, and at 1000 °C, the difference was 63.6 %. This is because, under high-temperature conditions, water cooling causes a rapid temperature drop in the concrete, generating significant thermal stresses. The rapid cooling induces microcracks at the interface between the steel fibres and the matrix. Additionally, due to the high thermal expansion coefficient of steel fibres, rapid cooling causes them to contract quickly, producing additional stresses and interface separation from the concrete matrix. High temperatures also cause grain coarsening in steel fibres, reducing their strength and toughness along with diminishing their reinforcing effect in concrete, especially

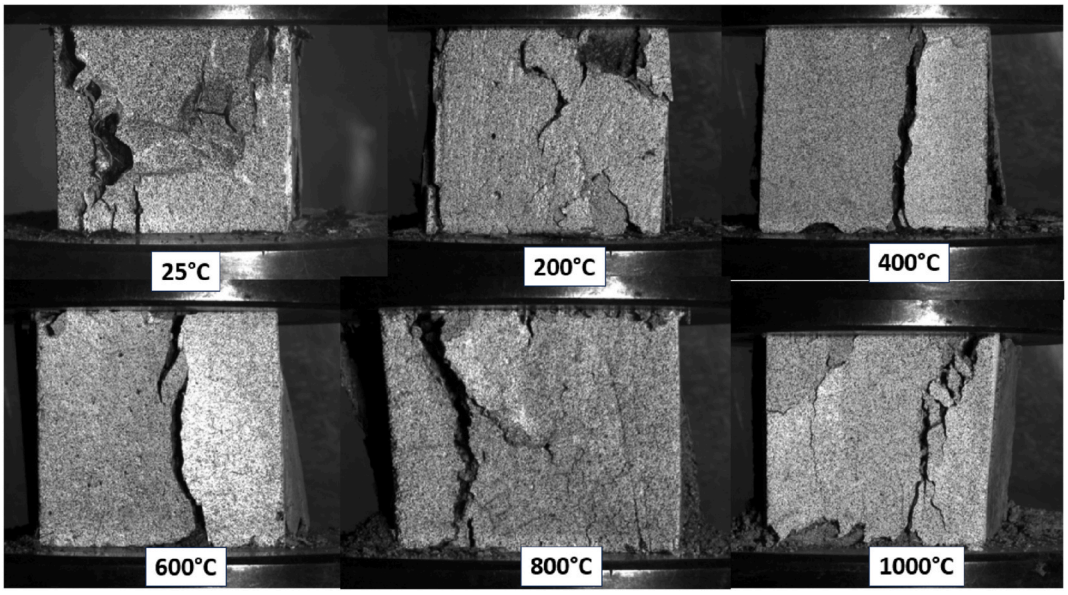


**Fig. 14.** Failure modes of GUHPC cooled down in air.

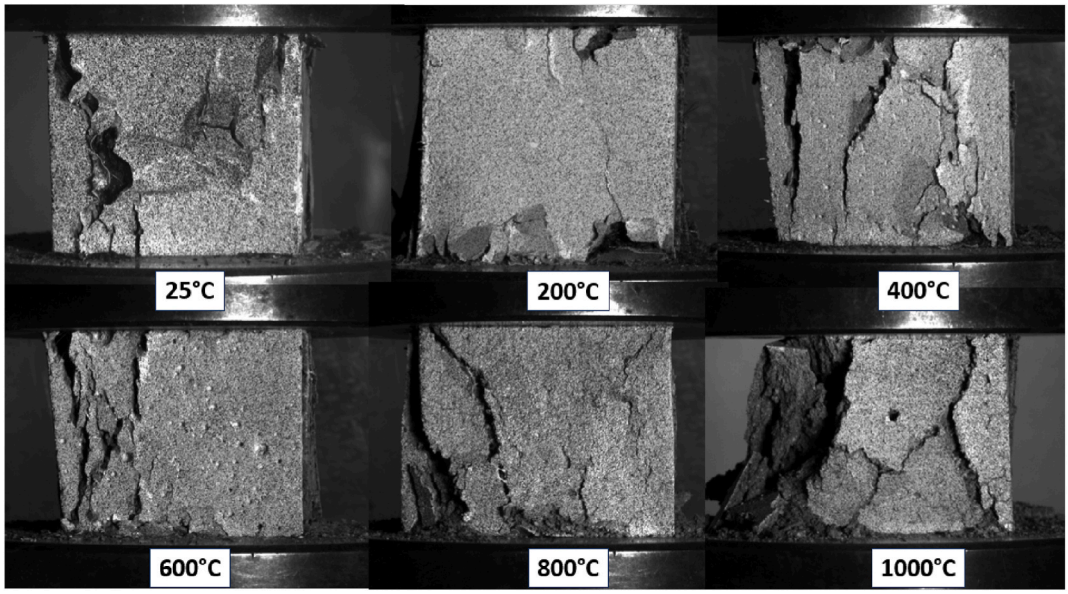


**Fig. 15.** Typical failure modes of GUHPC cooled down in water.

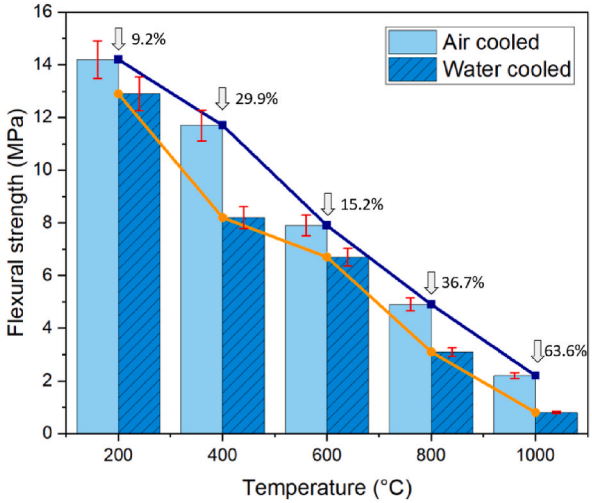


**Fig. 16.** Comparison of flexural strength between two cooling methods.

**Table 9**
Flexural strength of GUHPC at different temperatures with cooling methods.

| Temperature (°C) | $\sigma f_{AC}$(MPa) | $\sigma f_{WC}$ (MPa) | $RS_{AC}$ (%) | $RS_{WC}$ (%) |
|---|---|---|---|---|
| 25 | 16.1 | 16.1 | 100.0 | 100.0 |
| 200 | 14.2 | 12.9 | 88.2 | 80.1 |
| 400 | 11.7 | 8.2 | 72.7 | 50.9 |
| 600 | 7.9 | 6.7 | 49.1 | 41.6 |
| 800 | 4.9 | 3.1 | 30.4 | 19.3 |
| 1000 | 2.2 | 0.8 | 13.7 | 4.9 |

Note: $\sigma f_{AC}$ is air cooled flexural strength; $\sigma f_{WC}$ is water cooled water cooled flexural strength; $RS_{AC}$ is the percentage of residual flexural strength after air cooling.; $RS_{WC}$ is the percentage of residual flexural strength after water cooling.

above 500 °C [59]. Since steel fibres play a more important role in enhancing the flexural performance of concrete, water cooling thus exhibits a pronounced impact on concrete flexural strength.

Fig. 17 shows the load-CMOD curves of GUHPC, which was generally divided into three stages.

(1) Pre-crack linear elastic phase: At the beginning of all curves, from the inception of loading to the onset of significant non-linearity, the curves were essentially straight or nearly straight. This indicated that the concrete exhibited almost linear elastic behaviour within this stage. The linearity was more pronounced in the samples at room temperature and 200 °C.
(2) Non-linear crack propagation phase: As cracks formed and propagated, the curves deviated from their linear sections and began to show non-linear behaviour. This stage corresponded to the slow propagation of bending cracks under gradually increasing loads, manifested as a curvature in the curves. For samples at higher temperatures, this phase occurred earlier, and the slope of the curve was lower due to the reduced strength of the material.
(3) Rapid crack propagation to failure phase: The declining trend following the peak of the curves corresponded to the third stage, where the main crack rapidly propagated until the failure of the specimen. For specimens around 25 °C and 200 °C, the curve declined gradually during this phase, indicating that steel fibres retained material integrity even as cracks began to propagate rapidly. However, at elevated temperatures, especially in specimens at 600 °C and 800 °C, there was an earlier onset of the rapid crack propagation, coupled with a more precipitous decline in load-bearing capacity. This suggested a sudden failure of the material together with a substantial weakening of the bridging capabilities of steel fibres.

A comparison of cooling methods on GUHPC revealed that the damage level of water-cooled samples at 400 °C was comparable to that of air-cooled cases at 600 °C. This happened because the faster the cooling rate, the more damage occurred to the steel fibre. Water cooling, being a fast-cooling method, rapidly reduced the temperature and exacerbated the concrete material damage at high temperatures. That is, starting from 400 °C, the water-cooled specimens already exhibited increased strength loss and potential micro-damage due to the rapid cooling, causing more severe damage to both steel fibres and concrete matrix. In contrast, the air cooling represented a relatively gentle cooling process, with accumulated thermal stress and material damage becoming apparent at 600 °C.

### 3.3.2. *Toughness of fracture*

Fracture toughness is a key parameter for assessing the resistance of a material to crack extension which is usually calculated with the double-K fracture rule. This rule was described within the literature [60–62]. The initial fracture toughness, $K_{IC}^{Q}$, and the unstable fracture toughness, $K_{IC}^{S}$, are the key parameters in tracking the crack propagation behaviour within concrete. According to the double-K fracture rule, three phases based on stress intensity factor were described: No cracking occurred for the factor below $K_{IC}^{Q}$; between $K_{IC}^{Q}$ and $K_{IC}^{S}$, the crack grew in a stable manner; for the factor exceeding $K_{IC}^{S}$, the crack advanced unstably. Specifically, the initial fracture toughness was determined based on the response of concrete under initial crack load and notch depth conditions. The specific calculations are presented with Eqs. (4) and (5), which combine the initial crack parameters and material response to derive the resistance of GUHPC against crack extension at the initial stage. Further, $K_{IC}^{Q}$ of each specimen is based on the nonlinear initial point of its load-CMOD curve. This means that the fracture toughness can be assessed by analysing the relationship between load and CMOD, especially in the initial nonlinear portion of the curve.

$$K_{IC}^{Q} = \frac{1.5 \times \left(F_Q + \frac{mg}{2} \times 10^{-2}\right) \times 10^{-3} \times s \times a_0^{0.5}}{th^2} \times f(a) \tag{4}$$

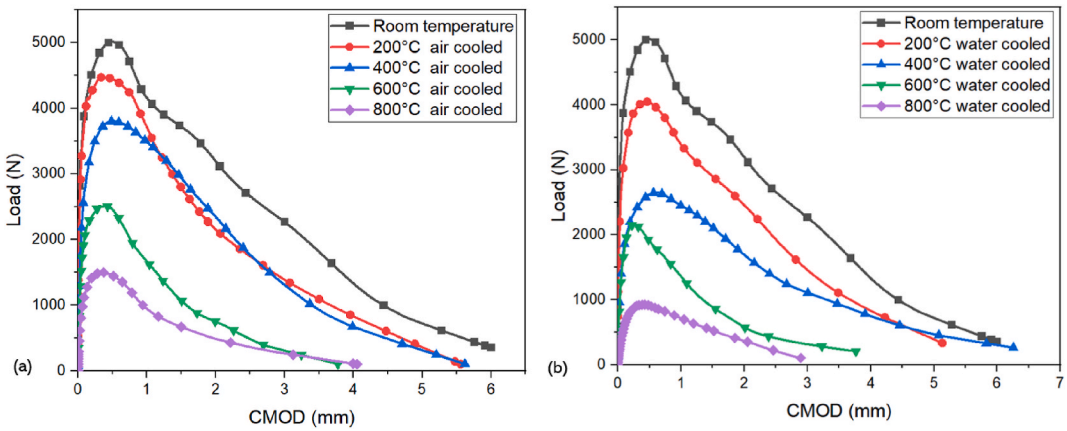


**Fig. 17.** Typical load-CMOD curves of GUHPC after (a) air cooled and (b) water cooled.

$$f(a)=\frac{1.99-a\times(1-a)\times(2.15-3.93a+2.7a^2)}{(1+2a)\times(1-a)^{1.5}},a=\frac{a_0}{h} \tag{5}$$

where $K_{IC}^{Q}$ is initial fracture toughness (MPa•m$^{0.5}$); $F_Q$ is initial crack load (kN); $a_0$ is initial notch depth (m); *S, h and t* are the span, height, and thickness of the beam (m), respectively; *g* is equal to 9.81 m/s$^2$; *m* is mass of the specimen (kg). The unstable fracture toughness calculation is presented with in Eqs. (6)–(8).

$$K_{IC}^{S}=\frac{1.5\times\left(F_{\max}+\frac{mg}{2}\times10^{-2}\right)\times10^{-3}\times s\times a_c^{0.5}}{th^2}\times f(a) \tag{6}$$

$$f(a)=\frac{1.99-a\times(1-a)\times(2.15-3.93a+2.7a^2)}{(1+2a)\times(1-a)^{1.5}},a=\frac{a_c}{h} \tag{7}$$

$$a_c=\frac{2}{\pi}h\times\arctan\sqrt{\frac{tE\times CMOD_c}{32.6\times P_{\max}}-0.1135} \tag{8}$$

where $K_{IC}^{S}$ is unstable fracture toughness (MPa•m$^{0.5}$); $F_{\max}$ is maximum load (kN); $a_c$ is critical crack length (m); CMODc is the critical crack mouth opening displacement corresponds to peak load (m); *E* is elastic modulus (MPa). Since DIC was used to measure CMOD, the influence of $h_0$ (thickness of the measure tool) is negligible, and it is excluded from the Eq. (8).

Eqs above are designed for fractured beams with a clear span-to-height ratio of 4.0. To adjust for different ratios, a correction coefficient K for $f(a)$, is applied as shown below as Eq (9).

$$K=1+\left(1-4\times\frac{h}{s}\right)\times\left[0.08\times\left(1-\frac{a}{h}\right)+0.24\times\left(1-\frac{a}{h}\right)^2-0.28\times\left(1-\frac{a}{h}\right)^3\right] \tag{9}$$

Table 10 and Fig. 18 present the fracture toughness of high-temperature GUHPC after air cooled and water cooled. The data only included test results in the temperature range of 25 °C–800 °C since concrete at 1000 °C basically lost its strength. Fig. 18(a) illustrates that the difference in the two cooling modes for initial fracture toughness at 200, 400, 600 and 800 C$^o$ was 13.9 %, 29.7 %, 36.6 % and 50 %, respectively, indicating that the initial fracture toughness was highly susceptible to the cooling regime. This may be due to changes in the internal microstructure of the material during cooling, such as the interfacial properties between the steel fibres and the concrete matrix, or the formation of microcracks and pores, which influenced the resistance of concrete to cracking. In contrast, the unstable fracture toughness exhibited in Fig. 18(b) reflected the performance of GUHPC during the rapid crack extension phase, with values of 3.2 %, 9.9 %, 12.9 % and 29.5 % variation at 200, 400, 600 and 800 °C. Once cracks formed in the concrete, the position and role of the steel fibres near the cracks became more stable. This stability allowed the fibres to bridge the cracks more effectively, providing sustained support and reinforcement. Consequently, the cooling method had less impact on further crack propagation, as the steel fibres already played their primary role during the initial crack formation.

### 3.3.3. Fracture energy

The fracture energy of three-point bending specimens is calculated by Eq. (9) [63].

$$G_f=\frac{W_0+mg\times\delta_c}{A_{lig}} \tag{10}$$

where $G_f$ is the fracture energy in the unit of N/mm; $W_0$ is the external work; *m* is the beam mass (kg); *g* is equal to 9.81 m/s$^2$; $\delta_c$ is the final mid-span displacement (mm) and $A_{lig}$ is the ligament area (mm$^2$).

Table 11 presents the difference in fracture energy of GUHPC at various temperatures using different cooling methods. The fracture energy of the GUHPC gradually decreased with increasing temperatures. At room temperature, steel fibres performed the best and consumed more energy during crack propagation owing to bridging effect, resulting in a value of 10.32 N/mm. However, as the temperature raised, the bonding effect between steel fibres and the concrete matrix deteriorated, leading to a reduction in fracture energy. Upon reaching 800 °C, steel fibres diminished in strength signally, resulting in a minimal fracture energy indicative of the greatly compromised material integrity. At the extreme temperature of 1000 °C, steel fibres carbonated and lost all their strength, with the fracture energy of GUHPC closing to zero. In conclusion, the mechanical strength of steel fibres within the concrete matrix deteriorated dramatically with an increase in temperature. Meanwhile, the gel structure in geopolymers changed under the impact of high temperatures, followed by thermal shock, causing its rupture. These variations consequently resulted in a reduction in the bonding of gel with steel fibres, which visibly diminished the fracture energy of GUHPC.

As provided by CEB-FIP Model Code 2010, Eq. (10) is the empirical formula to determine fracture energy.

$$G_f=73\times f_{cm}^{0.18} \tag{11}$$

where $G_f$ is fracture energy at room temperature (N/m) and $f_{cm}$ is concrete cylindrical compressive strength (MPa).

It is noteworthy that the foregoing formula is for ordinary concrete and does not present the variation in fracture energy after high temperatures. Therefore, this study proposed a new empirical Eq. (11) based on linear fitting of the experimental data. The values of

**Table 10**
Fracture toughness of GUHPC (MPa•m$^{0.5}$).

| Temperature (°C) | $K_{IC}^{Q}$ AC | $K_{IC}^{S}$ AC | $K_{IC}^{Q}$ WC | $K_{IC}^{S}$ WC |
|---|---|---|---|---|
| 25 | 1.34 | 12.74 | 1.34 | 12.74 |
| 200 | 1.13 | 10.55 | 0.97 | 10.21 |
| 400 | 0.89 | 10.03 | 0.63 | 9.04 |
| 600 | 0.70 | 8.94 | 0.44 | 7.78 |
| 800 | 0.35 | 7.74 | 0.18 | 5.46 |

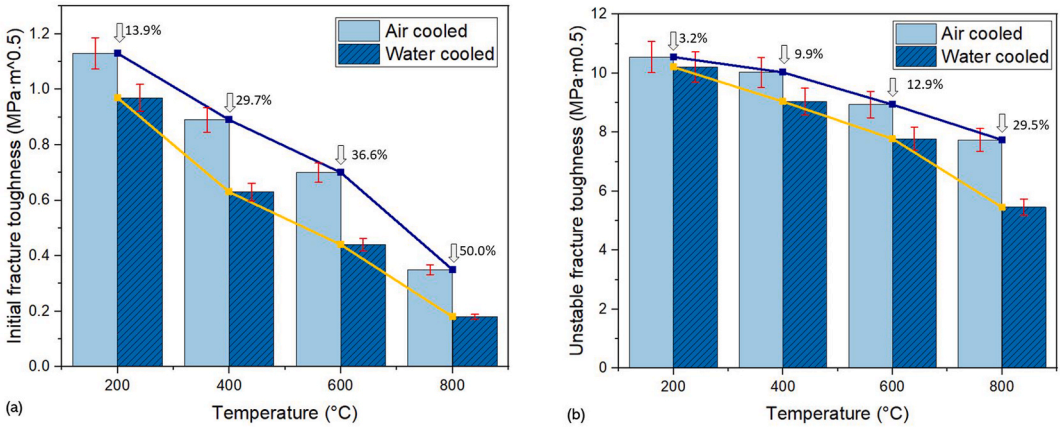


**Fig. 18.** Differences of (a) initial fracture toughness and (b) unstable fracture toughness between water cooled and air cooled.

**Table 11**
Fracture energy of GUHPC (N/mm).

| Temperature (°C) | Air cooled | Water cooled |
|---|---|---|
| 25 | 10.32 | 10.32 |
| 200 | 7.64 | 7.43 |
| 400 | 6.96 | 5.57 |
| 600 | 2.79 | 2.34 |
| 800 | 1.86 | 1.13 |

coefficient a are listed in Table 12.

$$G_f = a \times 10 \times f_c^{1.43} \tag{12}$$

where $G_f$ is the fracture energy of GUHPC at different temperatures (N/m); $a$ is the reduction coefficient at different temperatures; $f_c$ is the cubic compressive strength of GUHPC at 25 °C (MPa).

### 3.3.4. *Failure characteristics*

The typical flexural failure modes of GUHPC samples after thermal damage are exhibited in Figs. 19 and 20. The specimens from room temperature up to 800 °C demonstrated a certain degree of bending resistance with certain ductility. However, when the temperature reached 1000 °C, steel fibres completely carbonised and lost their strength, resulting in a loss of bending resistance in GUHPC with insignificant ductility after cracking. This set of results highlighted the critical influence of the steel fibres on the flexural behaviour of GUHPC, especially at high temperatures where the carbonation phenomenon had a serious impact on bending ductility.

**Table 12**
Value of $a$ for GUHPC fracture energy after high temperatures.

| Temperature (°C) | Air cooled | Water cooled |
|---|---|---|
| 25 | 1.0 | 1.0 |
| 200 | 0.74 | 0.71 |
| 400 | 0.67 | 0.54 |
| 600 | 0.27 | 0.23 |
| 800 | 0.18 | 0.11 |

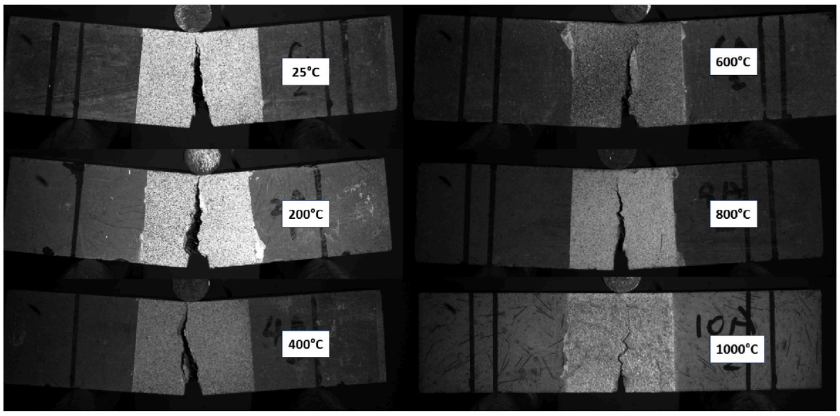


**Fig. 19.** Typical flexural failure patterns of GUHPC cooled down in air.

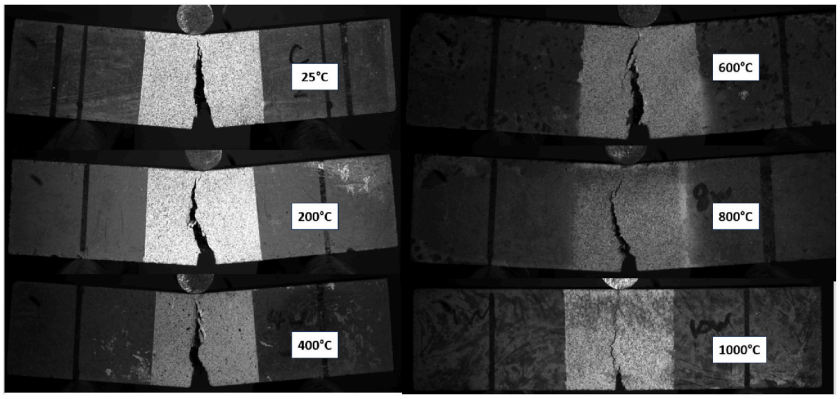


**Fig. 20.** Typical flexural failure patterns of GUHPC cooled down in water.

At room temperature, the samples demonstrated relatively clean fracture surfaces. Under the air-cooling condition (Fig. 19), the samples exhibited some irregularities in the fracture surface at 200 °C and 400 °C, indicating that the increase in temperature led to certain internal changes within the concrete matrix such as water evaporation and development of microcracks. When the temperature reached 600 °C and 800 °C, fracture surface was rougher and the significant cracking and spalling were observed, suggesting that the higher temperatures caused severe damage to the structure of concrete and affected its matrix properties. Upon reaching the critical temperature of 1000 °C, a notably rugged fracture texture with multiple cracks was observed, which indicated that the heated GUHPC lost a majority of its structural integrity and load-bearing capacity.

For the water-cooling regime as depicted in Fig. 20, the specimen demonstrated a more direct fracture surface, albeit with minor irregularities at 200 °C. This suggested that the effect of water cooling on GUHPC was still limited. As the temperature raised to 400 °C, fracture surface became rougher. GUHPC exhibited a more complex fracture surface between 600 °C and 800 °C, with cracks propagating in multiple directions, indicating that more microcracks and defects were present inside concrete. At an elevated temperature of 1000 °C, very rough and irregular fracture surfaces accompanied by a large number of spalls and cracks were observed, which could be attributed to material damage caused by the very high temperatures and the rapid temperature changes caused by water cooling. Rapid cooling usually led to the greater thermal stress within the matrix, developing more cracks and defects and eventually affecting the mechanical property of concrete itself. Especially under high temperature conditions, water cooling exacerbated the degradation of concrete properties.

It is noteworthy that the inclusion of steel fibres enhanced the crack resistance and toughness of GUHPC and therefore the concrete performance deteriorated more slowly than that of non-reinforced concrete at elevated temperatures. Nevertheless, at the extreme-high temperatures, GUHPC still exhibited a remarkable degradation in structural performance.

### *3.4. Microstructural analysis*

#### *3.4.1. SEM analysis*

Fig. 21 shows the typical microstructure of GUHPC at ambient temperature. The concrete still contained incompletely reacted FA, but the geopolymer matrix remained intact. The highlighted particles indicated the geopolymerization products in which the presence

of tiny cracks could be found, which was likely attributed to the fact that GUHPC was inherently porous in structure. The steel fibres at room temperature were observed as smooth and intact with no cracks on their surfaces. The concrete gel layer attached to the steel fibres indicated a good interfacial bonding between the concrete matrix and fibres. This bond was achieved through physical occlusion and chemical bonding at the microscopic level, which further ensured the integrity and stability of the concrete structure when subjected to forces. Effective bonding not only guaranteed force transfer at the microscopic level, but also signified that the steel fibres were distributing stresses and decelerating the progression of crack development in initial cracking phase, therefore impeding the transformation of the microcracks into more extensive macrocracks.

The effect of the cooling method on the microstructural characteristics of GUHPC at elevated temperatures was mainly reflected in the degree of damage to steel fibres. The SEM results exhibited in Fig. 22 indicated that the water cooling caused more severe damage to the steel fibres, which explained the greater decrease in flexural strength in comparison to compressive strength, attributing to the critical role of steel fibres in flexural performance. When rose to 800 °C, steel fibres began to exhibit varying degrees of carbonation. At 1000 °C, the fibres were completely carbonised with hardly any strength, turning into the powder when touched, along with no steel fibres observed in the SEM images. This also validates the analysis presented by the author in Section 3.3.1. Additionally, the amount of unreacted FA decreased with increasing temperature, and the destruction of FA was a contributing factor to the deterioration in strength.

For GUHPC, the microstructural changes after elevated temperature exposure were equally significant. High temperature led to dehydration and structural reorganisation of the geopolymer matrix, with SEM observations exhibiting microcracks and pore structural changes. The increase in cracks and porosity directly affected the various performance of GUHPC. In addition, the inorganic components, such as FA particles, also exhibited varying degrees of changes after subjected to different temperatures. At lower temperatures of no more than 200 °C, the changes were not evident. However, at 800 °C and above, the FA particles underwent the structural loosening or even partial melting, resulting in a notable decrease in the matrix strength of GUHPC.

### *3.4.2. XRD analysis*

Fig. 23 shows the XRD result of GUHPC after elevated temperature, in which AC stands for the air cooled and WC stands for the water-cooled conditions. Between 400 °C and 600 °C, GUHPC typically underwent the formation of mullite. Mullite generally originated from two sources: (i) from existing mullite ($3Al_2O_3 \bullet 2SiO_2$) present in the raw material that underwent structural changes at high temperatures; (ii) from the compounds containing calcium silicate (or sodium silicate) and aluminium, which experienced a process of the chemical rearrangement and crystallization at lower temperatures. In this temperature range, the strength of GUHPC was affected to some extent, but the temperatures were not sufficient to cause significant influences in the geopolymer structure. However, with temperatures further increased to 800 °C and 1000 °C, the new mineral phases such as gehlenite and akermanite appeared in the concrete. These phases were usually formed during the high-temperature chemical reactions such as decomposition and recrystallisation of pre-existing C(N)-A-S-H gels. The formation of the new phases at high temperatures could cause the decomposition of the original hydrated geopolymer products, thus weakening concrete performance. Moreover, the formation of akermanite and gehlenite was accompanied by remarkable volume changes, which led to an increase in the internal stress and the generation of microcracks and pores, thus reducing the mechanical properties of GUHPC.

The XRD patterns revealed that the characteristic peaks of the original mineral phases, such as and mullite, started to diminish or even disappear as the temperature raised, suggesting decomposition of the mineral phases. In addition, the hydration products, which played a crucial role in GUHPC property, underwent dehydration and chemical decomposition under high temperature conditions, further deteriorating the concrete's structural integrity and matrix properties.

Furthermore, during the heating, the microstructure of GUHPC underwent significant changes due to the phase transformation of various solid-phase substances such as the calcium aluminates hydrates in the temperature interval from 20 °C to 300 °C. The phase transformation, especially the complete dehydration and crystal structure transformation (e.g., the formation of Ackermann crystals) occurring in the temperature interval from 600 to 800 °C, resulted in a highly porous structure and gave rise to a significant mechanical degradation. Therefore, the temperature played a decisive role in the thermal deformation and transformation of specific components

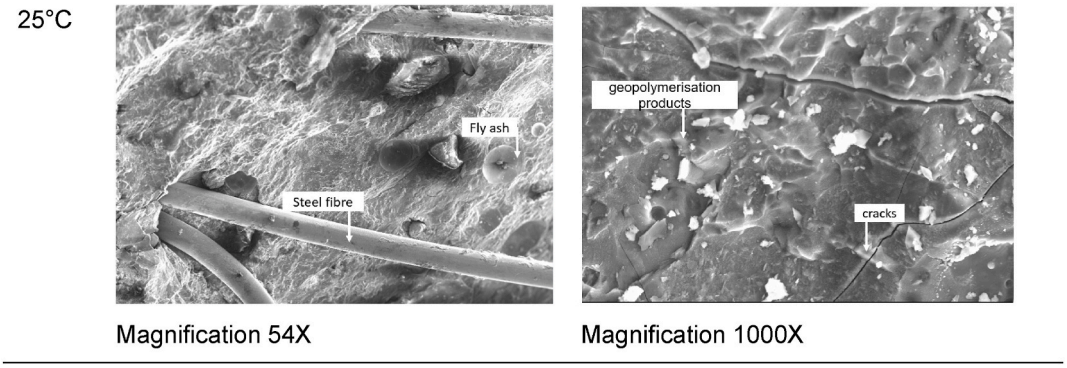


**Fig. 21.** Micromorphology of GUHPC at room temperature.

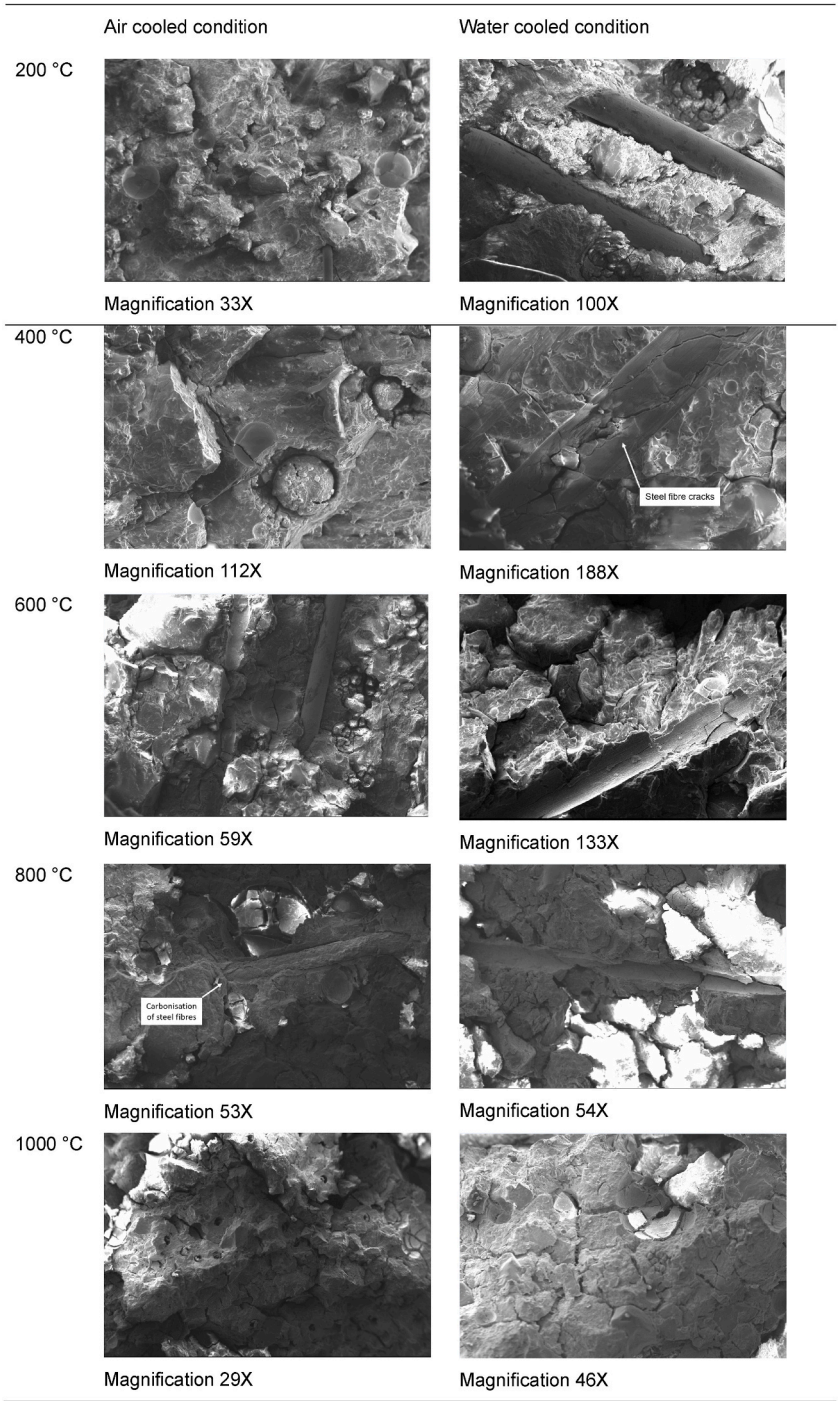


**Fig. 22.** Micromorphology of GUHPC at elevated temperatures.

in GUHPC.

In conclusion, under high-temperature conditions, GUHPC undergoes decomposition of hydration products, mineral phase transitions, and oxide reactions, all of which collectively influence its mechanical performance at elevated temperatures. As the temperature increases further to 600–1000 °C, gel completely decomposes, while any residual $CaCO_3$ undergoes thermal decomposition to produce CaO and $CO_2$ ($CaCO_3 \rightarrow CaO + CO_2$). Meanwhile, in a system rich in calcium oxide and alumina, gehlenite forms via the reaction of CaO, $Al_2O_3$, and $SiO_2$ ($2CaO + Al_2O_3 + SiO_2 \rightarrow Ca_2Al_2SiO_7$), while akermanite is generated from CaO, MgO, and $SiO_2$ ($2CaO + MgO + 2SiO_2 \rightarrow Ca_2MgSi_2O_7$).

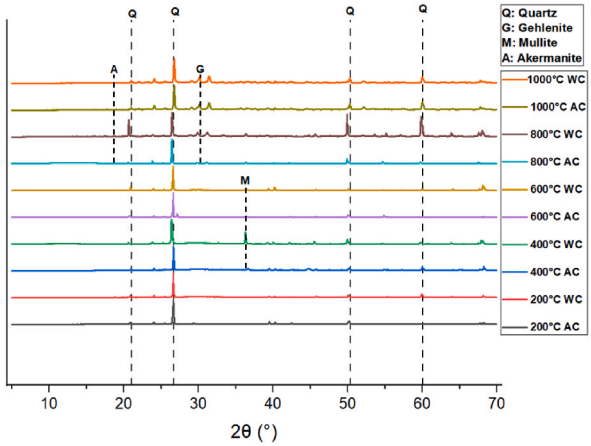


**Fig. 23.** XRD spectra of GUHPC after high temperature exposure.

## 4. Conclusions

From the experimental results of GUHPC exposed to high temperatures and different cooling methods, the following conclusions are summarized:

1) No indications of spalling were observed within the GUHPC matrix under high temperatures, which was likely attributed to the initial microcracks of GUHPC's characteristic that provided a channel for pore pressure release.
2) The post-temperature behaviour of GUHPC was characterized as three stages: Stage I from 25 °C to 200 °C, stage II from 400 °C to 600 °C, and stage III from 800 °C to 1000 °C, which corresponded to slight, moderate and notable declines in mechanical strength, respectively. At each stage, the residual strength can be roughly summarized as around 80 %, 50 %, and 20 % of the initial strength.
3) Water-cooling regime demonstrated a more significant impact on the flexural strength than compressive strength of GUHPC. For example, at the most severe strength loss stage at 1000 °C, the cooling method causes a 63.6 % difference in flexural performance and a 14.2 % difference in compressive performance. This was mainly attributed to the critical role that steel fibres played in augmenting the flexural performance of the concrete matrix.
4) The elastic modulus of GUHPC was approximately 10 % lower than that of CUHPC at ambient. The degradation effect of high temperatures on the elastic modulus, fracture toughness, fracture energy of GUHPC was also divided into three stages like its effect on compressive strength.
5) Exposure of GUHPC to a thermal environment of 400 °C instigated a solid-phase dehydration process, which caused an escalation in crack propagation, amplified porosity, coarsening of the pores and a subsequent diminishment in strength. Upon reaching a temperature of 600 °C, further occurrence of thermal cracking and phase decomposition led to a notable deterioration in the property of GUHPC. During 600–800 °C, GUHPC experienced the complete dehydration and phase decomposition, in which the unfavourable phase crystallization and transformation occurred, resulting in the development of porous microstructures.

GUHPC exhibits significant potential for extreme environmental applications due to its unique inorganic polymerization mechanism and high-temperature stability. However, compared to CUHPC, the thermochemical behaviour of GUHPC is more complex, as it is influenced by the type of geopolymer precursor, the choice of alkali activator, and the associated chemical reaction mechanisms. Variations in geopolymer compositions will lead to distinct microstructural transformations, phase transitions, and mechanical degradation patterns under elevated temperatures. Hence, investigating the residual performance of a specific GUHPC system after high-temperature exposure is vital for understanding its thermal stability and optimizing the refractory properties. The current study systematically analyses the residual mechanical properties and microstructural evolution of a selected GUHPC composite under elevated temperatures from 200 °C to 1000 °C, providing fundamental insights and crucial experimental data for the future development of more heat-resistant GUHPC formulations.

## CRediT authorship contribution statement

**Junjie Huang:** Writing – original draft, Methodology, Investigation, Formal analysis. **Jun Li:** Writing – review & editing, Supervision, Methodology, Conceptualization. **Ruizhe Shao:** Writing – review & editing, Supervision, Methodology, Conceptualization. **Chengqing Wu:** Writing – review & editing, Supervision, Resources, Methodology, Conceptualization.

## Declaration of competing interest

The authors declare that they have no known competing financial interests or personal relationships that could have appeared to

influence the work reported in this paper.

## Acknowledgement

This research is supported by the ARC Discovery Grant DP210101100. Appreciation is extended to UTS Tech Lab staff Benjamin Smith and PhD candidate Zizheng Yu for their valuable assistance during the experiments.

## Data availability

Data will be made available on request.

## References

[1] D. Wang, C. Shi, Z. Wu, J. Xiao, Z. Huang, Z. Fang, A review on ultra high performance concrete: Part II. Hydration, microstructure and properties, Constr. Build. Mater. 96 (2015) 368–377.
[2] R. Shao, C. Wu, J. Li, Z. Liu, Repeated impact resistance of steel fibre-reinforced dry UHPC: effects of fibre length, mixing method, fly ash content and crumb rubber, Compos. Struct. 321 (2023) 117274.
[3] J. Liu, C. Wu, Y. Su, J. Li, R. Shao, G. Chen, Z. Liu, Experimental and numerical studies of ultra-high performance concrete targets against high-velocity projectile impacts, Eng. Struct. 173 (2018) 166–179.
[4] F. Pacheco-Torgal, J. Castro-Gomes, S. Jalali, Alkali-activated binders: a review: Part 1. Historical background, terminology, reaction mechanisms and hydration products, Constr. Build. Mater. 22 (7) (2008) 1305–1314.
[5] N. Asim, M. Alghoul, M. Mohammad, M.H. Amin, M. Akhtaruzzaman, N. Amin, K. Sopian, Emerging sustainable solutions for depollution: geopolymers, Constr. Build. Mater. 199 (2019) 540–548.
[6] M. Abdellatief, M. Abd Elrahman, A.A. Abadel, M. Wasim, A. Tahwia, Ultra-high performance concrete versus ultra-high performance geopolymer concrete: mechanical performance, microstructure, and ecological assessment, J. Build. Eng. 79 (2023) 107835.
[7] Z. Huang, W. Chen, H. Hao, Z. Chen, T.M. Pham, T.T. Tran, M. Elchalakani, Flexural behaviour of ambient cured geopolymer concrete beams reinforced with BFRP bars under static and impact loads, Compos. Struct. 261 (2021) 113282.
[8] Z. Wang, E. Bai, B. Ren, Y. Lv, Effects of temperature and basalt fiber on the mechanical properties of geopolymer concrete under impact loads of different high strain rates, J. Build. Eng. 72 (2023) 106605.
[9] S. Xu, P. Yuan, J. Liu, Z. Pan, Z. Liu, Y. Su, J. Li, C. Wu, Development and preliminary mix design of ultra-high-performance concrete based on geopolymer, Constr. Build. Mater. 308 (2021) 125110.
[10] Y. Liu, C. Shi, Z. Zhang, N. Li, D. Shi, Mechanical and fracture properties of ultra-high performance geopolymer concrete: effects of steel fiber and silica fume, Cement Concr. Compos. 112 (2020) 103665.
[11] P. Song, Y. Liu, L. Kong, Z. Tang, G. Sun, Research on design and optimization for compositions of ultra-high-performance geopolymer concrete, J. Build. Eng. (2024) 111750.
[12] Y. Lin, C. Yang, H. Shi, Y. Wang, Z. Zong, H. Qian, S. Hou, S. Li, T. Chen, J. Cai, Dynamic mechanical properties of one-part ultra-high performance geopolymer concrete, J. Build. Eng. 95 (2024) 110173.
[13] M. Guerrieri, J. Sanjayan, F. Collins, Residual strength properties of sodium silicate alkali activated slag paste exposed to elevated temperatures, Mater. Struct. 43 (2010) 765–773.
[14] A. Rashad, Y. Bai, P.M. Basheer, N. Collier, N. Milestone, Chemical and mechanical stability of sodium sulfate activated slag after exposure to elevated temperature, Cement Concr. Res. 42 (2) (2012) 333–343.
[15] H.Y. Zhang, V. Kodur, B. Wu, J. Yan, Z.S. Yuan, Effect of temperature on bond characteristics of geopolymer concrete, Constr. Build. Mater. 163 (2018) 277–285.
[16] M. Rahmati, V. Toufigh, Evaluation of geopolymer concrete at high temperatures: an experimental study using machine learning, J. Clean. Prod. 372 (2022) 133608.
[17] I. Hager, Behaviour of cement concrete at high temperature, Bull. Pol. Acad. Sci. Tech. Sci. (1) (2013).
[18] Q. Zhang, G. Ye, Dehydration kinetics of Portland cement paste at high temperature, J. Therm. Anal. Calorim. 110 (1) (2012) 153–158.
[19] Y. Zhang, J.W. Ju, H. Zhu, Z. Yan, A novel multi-scale model for predicting the thermal damage of hybrid fiber-reinforced concrete, Int. J. Damage Mech. 29 (1) (2020) 19–44.
[20] Y. Zhang, S. Zhang, Q. Chen, Y. Shen, J.W. Ju, M. Bauchy, Insights into the effect of high temperature on the shear behavior of the calcium silicate hydrate by reactive molecular dynamics simulations, Int. J. Damage Mech. 31 (7) (2022) 1096–1112.
[21] Y. Chan, X. Luo, W. Sun, Compressive strength and pore structure of high-performance concrete after exposure to high temperature up to 800 C, Cement Concr. Res. 30 (2) (2000) 247–251.
[22] C. Castillo, Effect of Transient High Temperature on High-Strength Concrete, Rice University, 1987.
[23] Y. Zhang, S. Zhang, W. Zhao, Y. Wang, J.W. Ju, Z. Yan, H. Zhu, Spalling behavior in ultra-high performance concrete: multi-technique insights and multi-scale fiber-rubber mitigation strategies, J. Build. Eng. 98 (2024) 111333.
[24] M. Zeiml, D. Leithner, R. Lackner, H.A. Mang, How do polypropylene fibers improve the spalling behavior of in-situ concrete? Cement Concr. Res. 36 (5) (2006) 929–942.
[25] J.-C. Liu, K.H. Tan, Y. Yao, A new perspective on nature of fire-induced spalling in concrete, Constr. Build. Mater. 184 (2018) 581–590.
[26] L. Li, P. Jia, J. Dong, L. Shi, G. Zhang, Q. Wang, Effects of cement dosage and cooling regimes on the compressive strength of concrete after post-fire-curing from 800 C, Constr. Build. Mater. 142 (2017) 208–220.
[27] Y. Zhao, C. Wang, M. Teng, J. Bi, Observation on microstructure and shear behavior of mortar due to thermal shock, Cement Concr. Compos. 121 (2021) 104106.
[28] Y.-H. Huang, S.-Q. Yang, Y.-S. Bu, Effect of thermal shock on the strength and fracture behavior of pre-flawed granite specimens under uniaxial compression, Theor. Appl. Fract. Mech. 106 (2020) 102474.
[29] G.-F. Peng, S.-H. Bian, Z.-Q. Guo, J. Zhao, X.-L. Peng, Y.-C. Jiang, Effect of thermal shock due to rapid cooling on residual mechanical properties of fiber concrete exposed to high temperatures, Constr. Build. Mater. 22 (5) (2008) 948–955.
[30] W. Botte, R. Caspeele, Post-cooling properties of concrete exposed to fire, Fire Saf. J. 92 (2017) 142–150.
[31] Y. Zhai, Y. Li, Y. Li, S. Wang, Y. Liu, K.-I. Song, Impact of high-temperature-water cooling damage on the mechanical properties of concrete, Constr. Build. Mater. 215 (2019) 233–243.
[32] K. Liu, J. Liu, J. Li, M. Tao, C. Wu, Experimental investigation of heating–cooling effects on the mechanical properties of geopolymer-based high performance concrete heated to elevated temperatures, Structures (2023) 47.
[33] P. Rovnaník, P. Bayer, P. Rovnaníková, Characterization of alkali activated slag paste after exposure to high temperatures, Constr. Build. Mater. 47 (2013) 1479–1487.
[34] Y. Liu, X. Hu, Y. Du, B. Nematollahi, C. Shi, A review on high-temperature resistance of geopolymer concrete, J. Build. Eng. (2024) 111241.

[35] M.Z.N. Khan, Y. Hao, H. Hao, F.U.A. Shaikh, Mechanical properties of ambient cured high strength hybrid steel and synthetic fibers reinforced geopolymer composites, Cement Concr. Compos. 85 (2018) 133–152.
[36] M.Z.N. Khan, Y. Hao, H. Hao, F.U.A. Shaikh, K. Liu, Mechanical properties of ambient cured high-strength plain and hybrid fiber reinforced geopolymer composites from triaxial compressive tests, Constr. Build. Mater. 185 (2018) 338–353.
[37] X. Liang, C. Wu, Y. Su, Z. Chen, Z. Li, Development of ultra-high performance concrete with high fire resistance, Constr. Build. Mater. 179 (2018) 400–412.
[38] Z. Keshavarz, D. Mostofinejad, Effects of high-temperature exposure on concrete containing waste porcelain coarse aggregates and steel chips, J. Build. Eng. 29 (2020) 101211.
[39] K. Liu, C. Wu, X. Li, M. Tao, J. Li, J. Liu, S. Xu, Fire damaged ultra-high performance concrete (UHPC) under coupled axial static and impact loading, Cement Concr. Compos. 126 (2022) 104340.
[40] A.S. Carey, I.L. Howard, A. Knizley, J. Shannon, Modeling convection boundary conditions for ultra-high-performance concrete in cylindrical columns, ACI Mater. J. 117 (3) (2020) 123–131.
[41] ASTM C109, A, Standard Test Method for Compressive Strength of Hydraulic Cement Mortars (Using 2-in. Or [50-mm] Cube Specimens), American Society for Testing and Material, 2002.
[42] A. Astm, C78/C78M-18 Standard Test Method for Flexural Strength of Concrete Using Simple Beam with Third-point Loading, ASTM International, West Conshohocken, 2018.
[43] W.G.V. Saavedra, R.M. de Gutiérrez, Performance of geopolymer concrete composed of fly ash after exposure to elevated temperatures, Constr. Build. Mater. 154 (2017) 229–235.
[44] O. Rivera, W. Long, C. Weiss Jr., R. Moser, B. Williams, K. Torres-Cancel, E. Gore, P. Allison, Effect of elevated temperature on alkali-activated geopolymeric binders compared to portland cement-based binders, Cement Concr. Res. 90 (2016) 43–51.
[45] D.L. Kong, J.G. Sanjayan, Effect of elevated temperatures on geopolymer paste, mortar and concrete, Cement Concr. Res. 40 (2) (2010) 334–339.
[46] F. Qu, W. Li, Z. Tao, A. Castel, K. Wang, High temperature resistance of fly ash/GGBFS-based geopolymer mortar with load-induced damage, Mater. Struct. 53 (2020) 1–21.
[47] Y. Li, E.-H. Yang, K.H. Tan, Effects of heating followed by water quenching on strength and microstructure of ultra-high performance concrete, Constr. Build. Mater. 207 (2019) 403–411.
[48] H.Y. Zhang, G.H. Qiu, V. Kodur, Z.S. Yuan, Spalling behavior of metakaolin-fly ash based geopolymer concrete under elevated temperature exposure, Cement Concr. Compos. 106 (2020) 103483.
[49] Y. Zhang, Z. An, Y. Chen, W. Zhao, Z. Yan, H. Zhu, Revealing the role of multi-scale fibers in the compressive behavior of a novel ultra-high performance concrete subjected to elevated temperatures, Constr. Build. Mater. 447 (2024) 138127.
[50] K. Liu, C. Wu, X. Li, J. Liu, M. Tao, J. Fang, S. Xu, The influences of cooling regimes on fire resistance of ultra-high performance concrete under static-dynamic coupled loads, J. Build. Eng. 44 (2021) 103336.
[51] D.-Y. Yoo, J.-H. Lee, Y.-S. Yoon, Effect of fiber content on mechanical and fracture properties of ultra high performance fiber reinforced cementitious composites, Compos. Struct. 106 (2013) 742–753.
[52] Z. Wu, C. Shi, W. He, D. Wang, Uniaxial compression behavior of ultra-high performance concrete with hybrid steel fiber, J. Mater. Civ. Eng. 28 (12) (2016) 06016017.
[53] R. Shao, C. Wu, J. Li, Z. Liu, Investigation on the mechanical characteristics of multiscale mono/hybrid steel fibre-reinforced dry UHPC, Cement Concr. Compos. 133 (2022) 104681.
[54] R. Shao, C. Wu, J. Li, Z. Liu, Development of sustainable steel fibre-reinforced dry ultra-high performance concrete (DUHPC), J. Clean. Prod. 337 (2022) 130507.
[55] A. Hassan, M. Arif, M. Shariq, Use of geopolymer concrete for a cleaner and sustainable environment–A review of mechanical properties and microstructure, J. Clean. Prod. 223 (2019) 704–728.
[56] S.M. Qaidi, D.S. Atrushi, A.S. Mohammed, H.U. Ahmed, R.H. Faraj, W. Emad, B.A. Tayeh, H.M. Najm, Ultra-high-performance geopolymer concrete: a review, Constr. Build. Mater. 346 (2022) 128495.
[57] Report on High-Strength Concrete, American Concrete Institute, 2010.
[58] B.A. Graybeal, B. Stone, Compression Response of a Rapid-Strengthening Ultra-high Performance Concrete Formulation. No. FHWA-HRT-12-065, Federal Highway Administration. Office of Infrastructure. Research and Development, United States, 2012.
[59] En, B. 1-2, Eurocode 2: Design of Concrete Structures-Part 1-2: General Rules-Structural Fire Design, European Standards, London, 2004, 2004.
[60] S. Xu, H.W. Reinhardt, Determination of double-K criterion for crack propagation in quasi-brittle fracture, Part I: experimental investigation of crack propagation, Int. J. Fract. 98 (2) (1999) 111–149.
[61] S. Xu, H.W. Reinhardt, Determination of double-K criterion for crack propagation in quasi-brittle fracture, Part III: compact tension specimens and wedge splitting specimens, Int. J. Fract. 98 (1999) 179–193.
[62] S. Xu, H.W. Reinhardt, Determination of double-K criterion for crack propagation in quasi-brittle fracture, Part II: analytical evaluating and practical measuring methods for three-point bending notched beams, Int. J. Fract. 98 (1999) 151–177.
[63] M. D'Essai, T. Mé, P. De La Rilem, Size-effect method for determining fracture energy and process zone size of concrete, Mater. Struct. 1 (1) (1990) 7.